efforts of only a small percentage of faculty (8.9%), but this matter requires monitoring.

There is currently little reason to be concerned about the effect of foreign students on the continuing capacity of U.S. engineering schools to provide training and produce research. On the contrary, evidence suggests that without foreign students and foreign-born faculty, U.S. engineering education would suffer considerable damage. Nevertheless, it may be desirable for universities, for broader policy reasons, to attract greater numbers of well-qualified U.S. citizens to graduate study in engineering, thereby reducing the current dependency on foreign graduate students.

REFERENCES AND NOTES

1. *Foreign Citizens in U.S. Science and Engineering: History, Status and Outlook* (National Science Foundation, Washington, DC, 1985), p. 157.
2. For details, see A. Russo ["Selection of a faculty sample for a survey of the impact of foreign graduate students on U.S. engineering education," *Report CDT-86/1* (Center for Development Technology, Washington University, St. Louis, MO, 1986)].
3. If 20 undeliverable faculty questionnaires are excluded, the response rate rises to 54.3%.
4. Differences in response rate occurred among disciplines; only 47.2% of the EE faculty responded, compared to 60.1% of ChE faculty. Of the 11 faculty strata, the fewest responses came from ChE (128). As a consequence of surveying all department chairpersons, the chairperson population in the QRI-3 category was roughly twice that of either the QRI-1 or the QRI-2 population. The smallest number of chairperson responses was in ChE (96).
5. *An Assessment of Research-Doctorate Programs in the United States: Engineering* (National Academy Press, Washington, DC, 1982).
6. *Eng. Educ.* 75 (no. 6), 324 (March 1985).
7. Several questions pertained to this time period (approximately September 1981 through August 1985).
8. The percentages of respondents who indicated either a shortage or few, if any, well-qualified U.S. applicants were as follows: QRI-1, 70.4%; QRI-2, 88.8%; and QRI-3, 90.4%.
9. Almost all the chairpersons (99%) indicated that foreign citizens are required to demonstrate proficiency in English as part of the graduate admissions process, usually by achieving some minimum grade on the Test of English as a Foreign Language, which is produced by the Educational Testing Service.
10. The MRI faculty (45.8%) are defined as those faculty members who, over the past 3 years, said that they spent 26% or more of their time on externally sponsored research. The LRI faculty (54.2%) are those who spent 25% or less of their time on externally sponsored research.

11. We thank A. Abdallah, B. Barber, T. Bergeron, S. Berhorst, W. Darby, T. Feichtinger, M. Glassman, M. Golladay, C. Partain, J. Paules, A. Russo, E. Singer, D. Strickland, R. Torstrick, D. Williams, and P. Yee for their contributions, and members of our project advisory for their time and assistance. We thank the engineering faculty and chairpersons who completed the questionnaires. Supported by National Science Foundation grant SRS-8315308.

Global Images of the Earth's Interior

ADAM M. DZIEWONSKI AND JOHN H. WOODHOUSE

The three-dimensional maps of the earth's interior now span regions from the bottom of the crust to the inner core of the earth. Although a wealth of new information on the dynamics of the earth has been discovered, the inner core offers the greatest surprise: it appears to be anisotropic with the axis of symmetry aligned with the axis of rotation.

THE PACE OF PROGRESS IN SEISMOLOGY HAS QUICKENED recently. Thirty years elapsed between the discovery of the fluid core by Oldham in 1906 and the discovery of the inner core by Lehmann; it took another 35 years for a rigorous proof that the inner core is solid (1). Only 2 years separate the publication of the first three-dimensional maps of the upper mantle (*2, 3*) and the presentation at the 1986 spring meeting of the American Geophysical Union of two independent results on the aspherical structure of the inner core (*4, 5*). (The terms "aspherical" and "asphericity" will be used as synonymous with "lateral heterogeneity"; the ellipticity of the figure due to rotation described by the hydrostatic equilibrium theory is considered implicitly.) Studies of the earth's aspherical structure have now matured to the point where some of the results can be confirmed by independent techniques and where important conclusions can be drawn by the intercomparison of different models.

The primary reason for this rapid development was the accumulation of a sufficient quantity of high-quality digital data from two global networks (*6*) that began operation in the mid-1970s and achieved their full strength by about 1980. Theoretical developments during the last three decades provided the framework of formal analysis, and the availability of computers, including supercomputers, made feasible the handling of immense amounts of data and the large-scale calculations necessary in three-dimensional problems. Reports (*7, 8*) demonstrated that certain functionals of the earth's structure reflecting its asphericity can be retrieved and mapped on a global scale.

If the internal properties of the earth were spherically symmetric, our planet would be tectonically dead. Both short (earthquakes and volcanoes) and long time scale (mountain building and sea-floor spreading) observations indicate that this is not the case. This dynamic behavior must be driven by lateral differences in temperature and density. However, the internal distribution of these parameters cannot be uniquely inferred from observations at the surface.

The velocities of compressional and shear waves depend on temperature and composition and, therefore, density. Seismologists can determine the variations in the wave speeds. Regional studies, addressing relatively shallow structures whose tectonic nature is understood, demonstrate that the hypothesis of linking high seismic velocities with low temperatures, and vice versa, is justified. High seismic velocities have been found under continental shields, older than 1 billion years with very low heat flow, whereas the material in the vicinity of mid-oceanic ridges has very low velocities at the same

The authors are professors of geophysics in the Department of Earth and Planetary Sciences, Harvard University, Cambridge, MA 02138.

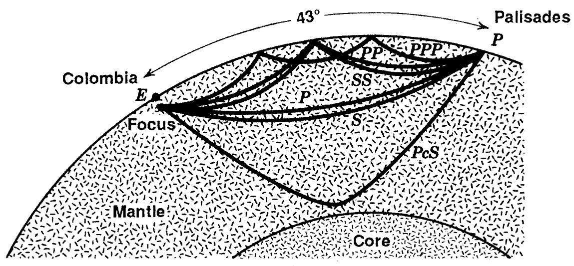

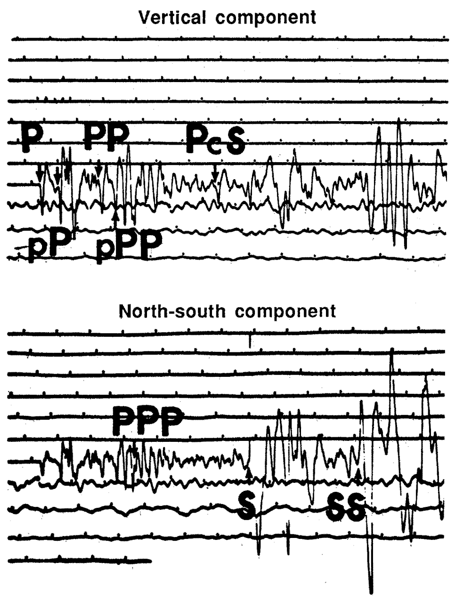

Fig. 1. Ray paths of seismic waves through the earth (left). The letter *P* corresponds to compressional waves and *S* to shear waves. Seismograms in which these phases were recorded are shown on the right. The use of information contained in such recordings ranges from reading of arrival times of various seismic phases to inversion of a complete, but usually low-pass filtered, wave train. Adapted from Donn (*22*).

depths. The extension of this hypothesis to depths greater than several hundred kilometers must rely on less direct inferences, such as correlation of the inferred velocity anomalies with the gravity field (*9, 10*). We have, therefore, good reasons to believe that by mapping seismological properties of the earth in three dimensions, we provide data that can answer some of the fundamental questions of geodynamics.

One such question is the driving mechanism of plate motions. Although the kinematic picture at the surface has been known for nearly 20 years, the views among geophysicists are still divided over how these motions translate with depth. Problems such as the existence of deep "continental roots" (*11*) or penetration of subducted material into the lower mantle (*12*) are examples of such issues.

Within the last year a new picture of the deepest region of the earth's interior, the core, has begun to emerge. At this stage various interpretations based on fragmentary information may appear to be mutually inconsistent. The three principal issues are the shape of the core-mantle boundary and properties of the material in its immediate vicinity, large-scale heterogeneity in the liquid core, and the existence of anisotropy in the solid inner core in addition to its isotropic properties that vary with position. The resolution of these issues is important to our understanding of the evolution of the earth, the generation and secular variation of the earth's magnetic field, and the thermal, mechanical, and chemical coupling between the core and the mantle.

The results obtained so far must be verified, and the proposed hypotheses must be tested against alternative explanations. The emergence of these problems, however, demonstrates the pace of change; as of 1 year ago no one was aware that the opportunity existed to address these questions.

This article reviews global seismic imaging, that is, the systematic, if rapid, progression away from the spherically symmetric earth models developed during the first three-quarters of this century. Equally important research being done on local and regional scales will not be discussed here. One can expect, however, that through increased resolution of global models and a broader application of regional studies the results of these two efforts can be combined, thus leading to a much improved understanding of how the earth works.

Mapping Infinity

The interior of the earth is inaccessible, but we can measure some of its functionals. A functional can be a complete seismogram or a single parameter derived from it, such as the arrival time of a *P*-wave. It is also possible to isolate a particular phase, such as a wave group of the fundamental Rayleigh (P-SV) or Love (SH) mode, and to estimate its dispersion. Another example of a functional is the location of a spectral peak corresponding to the frequency of a particular free mode of oscillation of the earth.

If the earth had a spherically symmetric structure and all sources were the same, for example, explosive pulses, then the shape of a seismogram would not depend on the location of the source or receiver but only on the distance between them. This simple relation is disturbed by the introduction of asphericity.

A perturbation due to aspherical earth structure of its functional, γ, can be expressed to the first order:

$$\delta\gamma = \int_V \boldsymbol{\delta}\mathbf{m}(\mathbf{x}) \cdot \mathbf{G}(\mathbf{x})dV \qquad (1)$$

where $\boldsymbol{\delta}\mathbf{m}(\mathbf{x})$ represents a vector of perturbations in elastic and anelastic parameters and density, and $\mathbf{G}$ is a differential kernel depending on the seismic source mechanism and the reference (spherically symmetric) earth's structure, and integration is over the entire volume V.

The problem can be simplified if the data are anomalies in travel times, δt, of body waves and the geometrical ray theory is used:

$$\delta\gamma = \delta t(\mathbf{x}_e,\mathbf{x}_r) = \int_{\mathbf{x}_e}^{\mathbf{x}_r} \delta v(\mathbf{x}) \cdot G(s)ds \qquad (2)$$

where $\mathbf{x}_e$ and $\mathbf{x}_r$ are the coordinates of source and receiver and $\mathbf{x} = \mathbf{x}(\mathbf{x}_e,\mathbf{x}_r,s)$ is a point on the ray path at angular distance s from the epicenter and $\delta v(\mathbf{x})$ is the perturbation in the compressional or shear wave speed. Two approximations are made. One is that the perturbation in the functional is linear with respect to perturbation in the model parameters. The other is that the kernel $\mathbf{G}$, computed for the reference model, does not depend on lateral heterogeneity. In the case of travel times of body waves, this approximation is justified by Fermat's principle, but the assumption could be relaxed in subsequent iterations, where the ray path could be traced through the previously estimated model of lateral heterogeneity. The first assumption leads to errors of the second order in $\delta\mathbf{m}$, which is acceptable for perturbations of the order of several percent; its effect would also be diminished in subsequent iterations.

For the problem to become tractable the number of unknowns must be made finite; two different ways of discretizing the problem have been used. One is to divide the medium into a three-dimensional array of cells in each of which the perturbation is constant. Thus for the jth path, between the source and receiver:

$$\delta t_j = \sum_i \delta v_i G_{ij} \qquad (3)$$

The summation is nominally over all the cells, i, but G_{ij} vanishes for cells not encountered by the ray path, so the matrix G_{ij} is sparse. Depending on the number of unknowns, the resulting system of normal equations can be solved either exactly (*9*) or by using iterative, approximate matrix inversion methods (*13, 14*).

The second approach to discretization is to expand δv in terms of basis functions. In the case of spherical geometry, the natural expansion is in terms of spherical harmonics Y_l^m:

$$\delta v(r,\theta,\phi) = \sum_{k=0}^{K} \sum_{l=0}^{L} \sum_{m=-l}^{l} {}_kC_l^m f_k(r) Y_l^m(\theta,\phi) \quad (4)$$

where θ and ϕ are, respectively, colatitude and longitude, $f_k(r)$ are given functions of radius, and ${}_kC_l^m$ are the unknown coefficients. Equation 4 can be thought of as a spatially filtered version of the full representation. The matrix of coefficients resulting from the substitution of Eq. 4 into Eq. 2 is not sparse. This representation has been used in (*15*) and (*3*), for example.

The basis function representation is possibly more computationally intensive than the cell approach in its application to residuals of travel time data, but it is clearly superior for other types of data (for example, splitting of normal modes), and its systematic application should allow us to combine in a single inversion a variety of types of data. In general, for the waves of finite wavelength a volume integral (Eq. 1) is appropriate. Such a representation is necessary for normal modes whose wavelength is a sizable fraction of the earth's circumference.

Any proposed model should, in principle, be specified with an estimate of its errors. Standard errors of coefficients ${}_kC_l^m$ were given in (*15*), and Tanimoto (*16*) adapted for three-dimensional geometry the approach of Backus and Gilbert (*17*) to evaluation of resolving kernels.

One should be cautious, however, in trusting such estimates. The sources of error are difficult, or impossible, to quantify. In addition to frequently unknown systematic errors in the data, two sources of error are particularly troublesome: errors in theory and errors in model representation. The latter are more fundamental. If, for example, anisotropy is important, the models obtained assuming isotropy could be severely biased and their specified standard errors will be meaningless and misleading. Seismologists are still searching for the proper mathematical representation of the unknown physical properties of the earth's interior. It is important at this stage to explore the earth with data that sample it in a significantly different way and to compare the resulting models. This approach is being carried out, and the formulation of the hypothesis that the inner core is anisotropic (*18, 19*) is a direct outcome of the encountered discrepancy between the isotropic models based on splitting of normal modes (*5*) and travel times (*4*). Similarly, the discrepancy between relative roughness of the core-mantle boundary obtained from seismic data and its smoothness inferred from astronomical observations (*20*) could lead to a fundamental change in our perception of the nature of this interface.

The Data

In all cases the original sources of data are seismograms: the recordings of ground motion caused by an earthquake or explosion. For the most part, the research described here involves interpretation of these recordings. The arrival times of body waves, however, are reported in the *Bulletins of the International Seismological Centre* (BISC), and these are used without reference to the original seismograms (*21*).

Figure 1 (*22*) shows schematically the ray paths of different body wave phases and the corresponding seismogram in which some of them are identified. The arrival times of such phases are sent to ISC from more than 1000 globally distributed stations. The center associates these readings with seismic events and publishes a catalog of earthquakes on a monthly basis (albeit with a 2-year delay; quick epicenter determinations can be obtained within a few hours after a major event by dialing a computer at the National Earthquake Information Service of the U.S. Geological Survey). All contributed readings are published and then distributed on magnetic tape.

Fig. 2. Summary residuals for a source region centered on 57.5°S and 27.5°W. Upward pointing triangles represent positive residuals, indicating slower than average propagation; downward triangles correspond to paths faster than normal. The size of a symbol is proportional to the size of the anomaly. From (*15*).

Although the potential of BISC for studies of lateral heterogeneities was recognized relatively early (*23*), the data set may be confusing because of the low signal-to-noise ratio. Even when gross mistakes are rejected, the contribution to the variance of a single observation of reading errors and small-scale lateral heterogeneities is ten times as great as that due to heterogeneities with the wavelength greater than several hundred kilometers (*24*). Averaging is one way to demonstrate that the effect of large-scale lateral heterogeneities is discernible. Figure 2 is a map of "summary residuals" of P-wave arrival times (*15*). Travel-time anomalies from 70 earthquakes in a 5° by 5° area, representing a "source region," were averaged in "receiver regions" (3° in epicentral distance, 7.2° in azimuth). Only points derived from at least five observations are plotted. Significant areal consistency is present in the pattern observed in Africa and Antarctica. The introduction of summary residuals also allows us to minimize the effect of the uneven distribution of earthquakes and seismographic stations.

Although the reports of the arrival times of the P-wave are most numerous (nearly 2 million individual readings have been used in some studies) and reliable, BISC contain information on other phases. Among them are the core reflections, *PcP*, and phases traveling through the core: *PKP* and *PKIKP*. These phases can be used to study the structure of the core (*4, 25*) and core-mantle boundary (*26–28*). Attempts to use other phases included in BISC have also been reported (*29*).

Travel-time residuals are used to retrieve the three-dimensional structure by forming the equations of condition from Eq. 2 by using a parameterization such as in Eqs. 3 or 4. The difficulty rests largely in the selection of the number and distribution of parameters consistent with the imperfect sampling of the earth by rays connecting source-receiver cells and with the level of noise in the data.

Another kind of data used in three-dimensional analysis is that

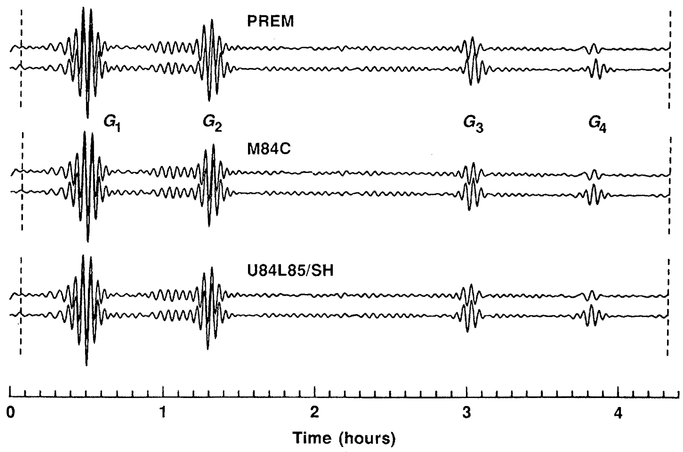

Fig. 3. Low-pass filtered observed and synthetic seismograms containing very long period waves ($f < 1/135$ Hz). The observed seismogram (top trace in each of the pairs) represents the transverse component (SH) of the ground motion and is obtained through rotation of two horizontal component recordings. The symbols G_n identify the consecutive arrivals of the fundamental mode of Love waves; the wave groups G_3 and G_4 have traveled more than one complete circumference of the earth. The bottom trace in each pair is a theoretical seismogram computed for three different earth models. PREM (*45*) is a spherically symmetric model that does not match well the observations for this path; the difference between the observed and the synthetic traces is used as input in inversion for a laterally heterogeneous earth model. The match between observations and model predictions is improved for the bottom two pairs. Model M84C (*3*) was derived by using approximately 2000 seismograms such as shown here; model U84L85/SH (*46*) was obtained by using, in addition, waveforms of body waves. (See Fig. 5.) The recording was made at Charters Towers, Australia, at a distance of 122.4° from an earthquake of magnitude $M_s = 6.4$ located on the South Atlantic ridge.

contained in very long period recordings. The top trace in Fig. 3 shows 4.5 hours of the transverse component record. The dominant features are bursts of energy associated with the fundamental mode Love waves traveling along world-circling paths. Such long-period data are used in four distinct ways.

Wave group approach. Individual wave groups are isolated and their phase velocity dispersion is estimated within a range of frequencies. By analyzing G_1, one obtains the dispersion along the minor arc (short path between the source and receiver), and G_2 yields dispersion along the major arc; G_3 corresponds to the travel along the minor arc and one full earth circumference. The method requires knowledge of the earthquake mechanism. The range of frequencies for which reliable estimates of dispersion can be obtained limits the resolution of the method to the top several hundred kilometers of the mantle.

Such data, obtained for many crisscrossing paths, could be directly substituted in Eq. 2, each measurement corresponding to a different functional γ. In the published reports, however, three-dimensional models have been obtained in two steps. First, the data were inverted for the spherical harmonic coefficients of phase velocity C_l^m (ω) at several discrete frequencies (*30*). Then the frequency dependence for each l and m was inverted for a function of depth, yielding the model (*2, 31*); these particular studies allowed for transverse (*32*) and azimuthal anisotropy (*33*). Recently, Tanimoto (*34*) incorporated the wave groups X, which represent the superposition of several overtones of surface waves (*35*); this improved the depth resolution of the wave group approach.

Asymptotic normal mode approach. If a record such as that shown in Fig. 3, but perhaps several times longer, is transformed into the frequency domain, the amplitude spectrum will show distinct peaks, which represent the interference of waves traveling on the sphere. In theory, for a rotating, elliptical, or, in general, aspherical earth, each mode of angular order l will be split into $2l + 1$ spectral lines (*36*). However, in the asymptotic limit of large l, propagation of energy is

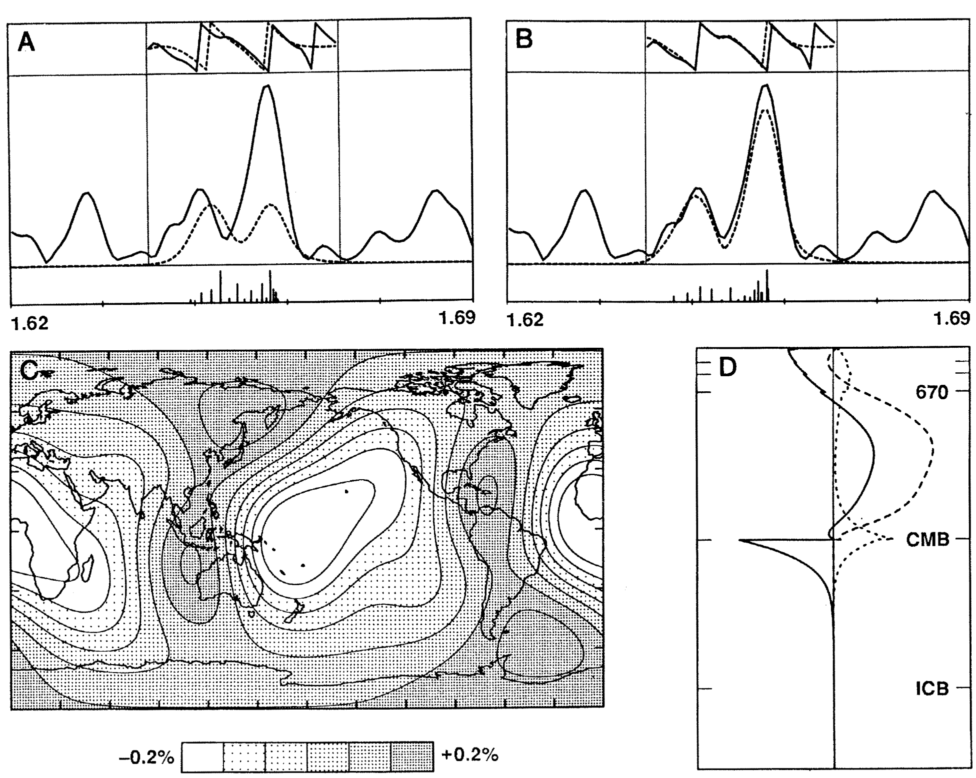

Fig. 4. (**A**) Phase (top) and amplitude (middle) of the mode ${}_1S_7$ compared with the prediction (dashed line) for a spherically symmetric earth model with consideration of the effects of rotation and ellipticity. The frequency and amplitude of the 15 theoretically predicted spectral lines are shown at the bottom. The horizontal scale is frequency in millihertz. The spectrum was derived from 120 hours of recording at Halifax, Nova Scotia, of a magnitude 8.3 earthquake in Indonesia. (**B**) Same as (A), but calculations are made considering aspherical perturbations described by the splitting function. (**C**) Splitting function for mode ${}_1S_7$ derived from simultaneous inversion of 38 spectra, such as in (A) and (B). The values describe relative perturbations in "local eigenfrequency" (*37*): the degenerate frequency of a spherically symmetric earth with the structure along the radius intersecting the surface at a given point. Only the spherical harmonics of degrees 0, 2, and 4 are recovered. (**D**) Sensitivity of local eigenfrequency with respect to perturbations in the density (solid line), compressional (dotted line), and shear velocity (dashed line) as a function of radius. Mode ${}_1S_7$ is sensitive to the structural parameters near the top of the outer core. Theoretically, the sensitivities depend on the harmonic degree of heterogeneity; for ${}_1S_7$, however, the kernels are similar for degrees 0, 2, and 4; therefore, only degree 0 is shown. ICB is inner-outer core boundary. After Giardini *et al.* (*43*).

limited to the great circle path through the source and receiver. Instead of appearing to be split, spectral peaks are shifted in frequency by amounts corresponding to the mean deviation from the spherical average of the structure along the great circle (*37*). Because the phase information is destroyed, the measurement is sensitive only to the even degrees of the earth's heterogeneity.

Masters *et al.* (*7*), using data from several hundred vertical component seismograms, measured frequency shifts for several thousand spectral peaks of the fundamental spheroidal mode and discovered that the pattern is dominated by degree 2.

Complete normal mode approach. The full set of $2l + 1$ lines can be readily retrieved only for a few modes. The problem is that spectral lines have finite width because of attenuation, and for the most part the separation of singlets is insufficient to retrieve the fine structure through direct inspection of individual spectra. Splitting of the "football" mode of ${}_0S_2$, with a period of 54 minutes, has been detected in the first reports on the observation of normal modes of the earth (*38*). This splitting has been explained, by Backus and Gilbert (*36*) and by Pekeris *et al.*, through the Coriolis effect, which is large at the lowest frequencies; later, the effect of the earth's ellipticity was theoretically predicted by Dahlen (*36*). The full set of singlet frequencies has also been reported for ${}_0S_3$ (*39*).

Masters and Gilbert (*40*) discovered that a mode ${}_{10}S_2$ was split 2.5 times more often than was predicted by the effect of rotation and ellipticity. This is a mode with properties similar to the *PKIKP* phase of the body waves (*41*); it has low attenuation and, therefore, relatively narrow spectral lines, which eases detection of the effect. Such anomalously large splitting has since been detected for a number of other modes with similar properties (*42, 43*). Estimation of the frequencies of individual spectral lines provides incomplete information on the heterogeneity. The effect is fully described by the splitting matrix, while the singlet frequencies are only its eigenvalues, which are invariant with respect to rotations.

Woodhouse and Giardini (*44*) proposed a procedure leading to the retrieval of the splitting matrix and the derivation of the splitting function, which has a geographical representation. The resulting map predicts values akin to the "local eigenfrequencies" (*37*), and these values represent linear constraints on structure. Figure 4, A and B, shows an example of observed and predicted spectra of the mode ${}_1S_7$ recorded at a station of the International Deployment of Accelerometers network at Halifax, Nova Scotia. The splitting function for this mode, derived through a simultaneous inversion of 38 spectra, is shown in Fig. 4C. The coefficients that describe such a function, except for estimation errors, represent objective information about the earth and are not burdened by the inaccuracies that may affect the results obtained from using various asymptotic methods. A shortcoming is that its resolution is limited to the retrieval of the even degrees, l, in Eq. 4. The splitting function is related to the earth structure through differential kernels, and such data for many modes with different properties can be inverted for laterally heterogeneous earth structure. Alternatively, the intermediate step can be bypassed, and the entire data set can be inverted directly. Giardini *et al.* (*43*) also explored this route; we refer to the model derived in that study as GLW.

Waveform approach. The low-pass filtered seismogram (cutoff frequency, 1/135 Hz), such as the one shown at the top of Fig. 3, can be represented by the superposition of approximately 600 normal modes, of which only 200 are of practical significance. Although the arrivals of the fundamental Love mode have the largest amplitudes, the trace between them is not flat, but it shows the energy of overtones, which propagate with different group velocities and whose sensitivity to structure is different from that of the fundamental mode. In procedures such as described in the wave group and the asymptotic normal mode approach sections above, this information is not used, and in fact is a source of error, since some of the energy of overtones is present within the time windows assigned to the wave groups G_1, G_2, and subsequent ones.

A spherically symmetric earth model [PREM (*45*)] does not predict well the observed arrivals for this particular path; G_3 is nearly 180° out of phase. Woodhouse and Dziewonski (*3*) developed an approach that allows the simultaneous use of all information contained in a seismogram within a selected time window. In their method, inversion for structural parameters ${}_kC_l^m$ (Eq. 4) is carried out by using complete seismograms such as those shown in Fig. 3 as data. The application of this procedure, by using only very long period data, led to the model M84C (*3*), which represents the upper mantle shear velocity expanded up to degree 8 in spherical harmonics and given as a cubic polynomial in radius. The prediction of this model is compared with the observation in the second pair of traces; the discrepancy has been removed.

The waveform approach is not limited to very long periods. Figure 5 shows observed body waves (cutoff, 1/45 Hz) for the same event and at the same station as in Fig. 3. The trace is truncated before the first arrival of surface waves. Such a trace consists only of overtones of normal modes, which are more sensitive to deeper structure. In other words, it contains information on a collection of rays such as those shown in Fig. 1; the sensitivity is, therefore, not only to a single ray path but, in effect, to the entire meridional cross section.

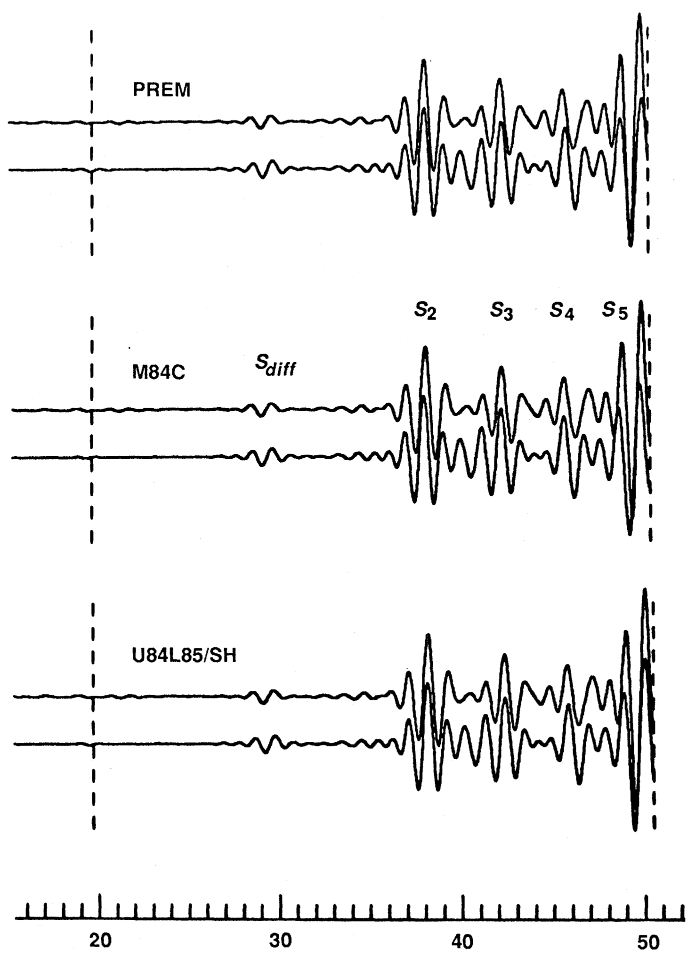

Fig. 5. Same as Fig. 3 but for long period body waves ($f <$ 1/45 Hz). The symbol S_{diff} identifies the S-wave diffracted at the core-mantle boundary; at a distance of 122.4° the station is in the core shadow for the direct S-wave arrival; S_2 is the phase SS (Fig. 1), S_3 is SSS and so on. Model U84L85/SH, of Woodhouse and Dziewonski (*46*), derived by using data such as shown in this figure, in addition to very long period data, predicts the observations better than M84C, which was obtained by using only the latter data source.

In addition, there are two other advantages of using body waves. Adequate signal-to-noise ratio can be achieved for events many times smaller than those producing discernible mantle waves. The ability to use smaller events leads to better geographical distribution of sources in regions without large earthquakes. Furthermore, the sensitivity to local structure is increased. The body wave seismograms are sensitive only to the minor arc structure, yet the greatest discrepancy in mantle wave data arises from differences in averages over complete great circles (even degree harmonics).

We derived model U84L85/SH (*46*) by using both mantle and body wave data. It predicts body waves better than model M84C, as shown by the last pair of traces in Fig. 5. It also predicts the mantle waves equally well (Fig. 3).

Maps of the Earth's Interior

The functionals described in the previous section contain information on all regions of the earth's interior. Their sensitivity to *P*- and *S*-velocities is depth-dependent. For example, the *P*-wave data used are limited to distances greater than 25° (which corresponds to the depth of a turning point of 750 km), because of highly nonlinear complications at shorter ranges. This means that their resolution of upper mantle structure is poor. Surface waves and other waveform data are primarily sensitive to the shear velocities in the upper mantle, although the incorporation of the waveform data for body waves (*46*) extended the resolving depth to about 1500 km. The elements of splitting matrices of normal modes depend on density and *P*- and *S*-wave speeds. With the existing data set, however, not all of these parameters can be resolved independently. We describe the current state of resolution of lateral heterogeneities in order of increasing depth.

Upper mantle. An important test of the validity of global imaging is that at shallow depths these studies yield results that are compatible with the tectonic expression at the surface as well as with regional scale investigations. A map of perturbation in shear wave velocity at a depth of 150 km is shown in the top of Fig. 6 for model U84L85/SH; at depths shallower than 400 to 500 km this model is similar to M84C (*3*). All shield areas are fast while mid-oceanic ridges are slow, in accordance with all the geophysical and geological evidence (*47*). This picture was obtained by using no previous information on the distribution of shields and mid-ocean ridges or the age of the oceanic lithosphere (old ocean basins are fast). It simply was retrieved through the inversion of several thousand seismograms by using the spherical harmonic expansion of Eq. 4 with the spherical harmonic degree limited to 8. This data set justifies expansion to higher degrees. Degree 8 corresponds to a resolving half-wavelength of 2500 km; Tanimoto (*16*) analyzed resolving kernels for a smaller data set and inferred a 2000-km resolving length.

The bottom part of Fig. 6 is a cross section through the upper mantle. It shows the depth expression of the differences between the shields and mid-oceanic ridges. The shields show large positive velocity contrasts (above 4%) down to a depth of about 200 km;

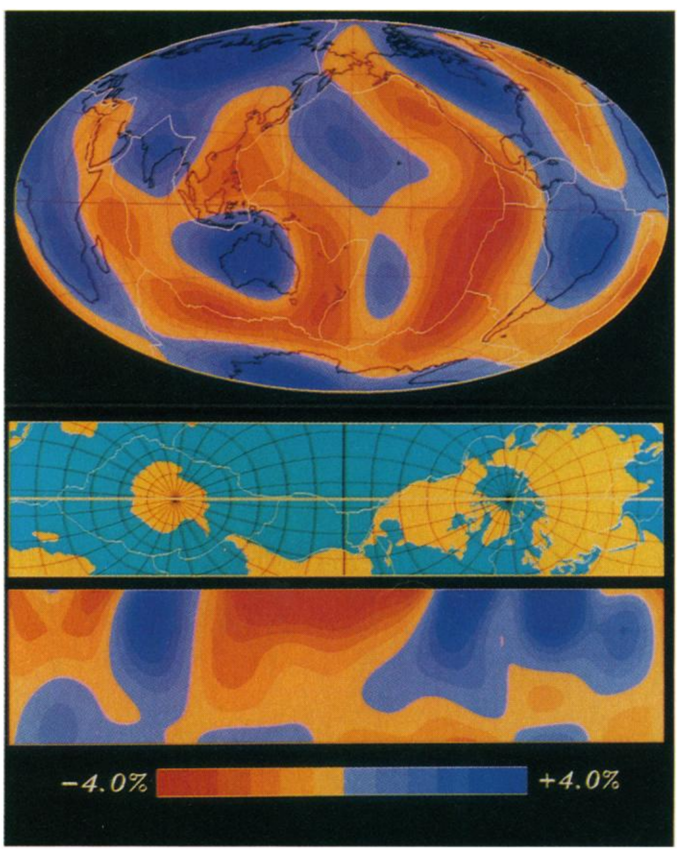

Fig. 6. Relative perturbations in the upper mantle shear velocities of model U84L85/SH (*46*). The map of the velocity anomalies at a depth of 150 km is shown in the top panel. White lines are the plate boundaries. The bottom panel is a cross section through the upper mantle (from Moho, at a depth of 26 km, to 670 km deep) along the meridian 110°W, shown as the thick center line in the map of the middle panel. The cross section reveals slow velocities under the mid-oceanic ridges and high velocities under continents. Vertical exaggeration is 20:1.

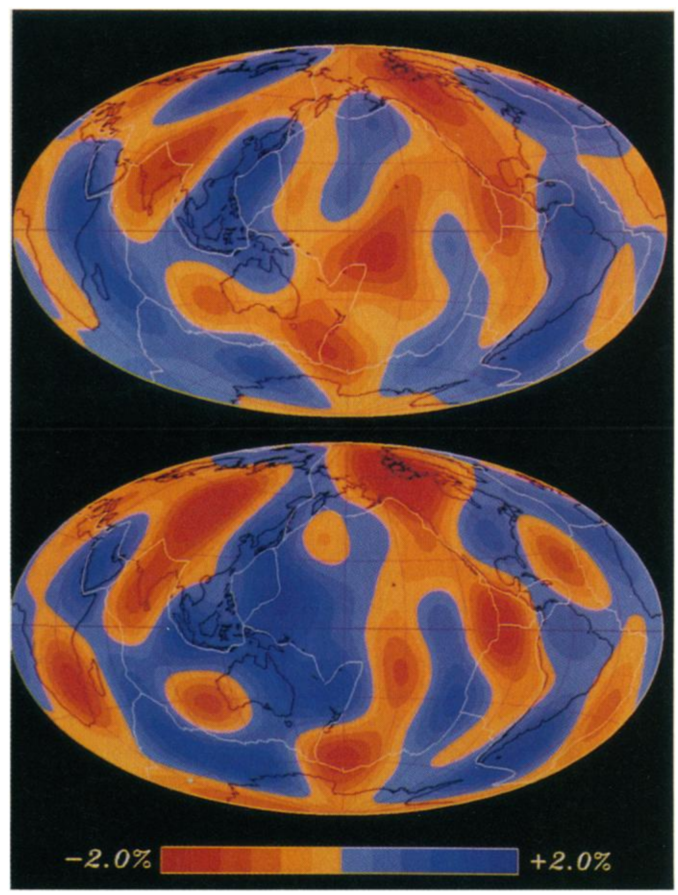

Fig. 7. Relative perturbations in the shear velocities just above (top) and below (bottom) the 670-km discontinuity, which is the boundary between the upper and lower mantle. The maps show substantial similarities even though the continuity was not explicitly demanded in the inversion: separate sets of coefficients describe the asphericity of the upper and lower mantle of model U84L85/SH of Woodhouse and Dziewonski (*46*).

this difference tapers off between 200 and 400 km and disappears completely in the transition zone (400 to 670 km). The depth expression of ridges is highly variable, with some reaching average velocities at about 200 km and others remaining anomalous as deep as 400 km.

The model from which Fig. 6 was derived was obtained from inversion of the combined data set of the transverse component body wave and mantle wave seismograms (*46*), thus consisting, in practice, only of SH motion. Unlike M84C (*3*), in which perturbations were confined to the upper mantle, an additional set of coefficients was derived for the lower mantle, with a discontinuity in the radial basis function representation at a depth of 670 km. A data set consisting of more than twice as many records of vertical and longitudinal components (P-SV) was also inverted by using the same parameterization, and it yielded a model that in the upper mantle is not conceptually different from the SH model. This seems to contradict, indirectly, the findings of Nataf *et al.* (*2*), who reported large differences between V_{SH} and V_{SV}. Clearly, the level of transverse anisotropy in the upper mantle needs to be investigated further.

The effect of azimuthal anisotropy (speed varies with the azimuth, rather than with the vertical angle of incidence, as in the transverse anisotropy) was investigated by Tanimoto and Anderson (*33*), who found similarities with the pattern of flow at the depth predicted from the velocities of plate motions (*48*).

The 670-km discontinuity. The existence of this discontinuity is well established (*49*). The subject of a debate, continuing now for about 20 years, is whether it represents a mineralogical phase change through which material may flow freely or whether it is an impenetrable chemical boundary separating the upper and lower mantle. The answer is significant to our understanding of the evolution and dynamic behavior of the earth. The subject remains controversial, as shown by the recent special session on the penetration of subducted slabs into the lower mantle held at an American Geophysical Union meeting (*50*). It was hoped that the question could be elucidated by a demonstration of the continuity or discontinuity of lateral heterogeneities at a depth of 670 km. The early aspherical models (*3, 15*) were disjoined at this depth, having been derived from two different data sets, each having the poorest resolution in this region.

With the incorporation of the long period body wave data the issue may now be approached. Figure 7 shows maps of *S*-velocity anomalies just above and just below the 670-km discontinuity: there is separate parameterization for the upper (U) and lower (L) mantle in model U84L85, and no explicit conditions on the continuity of the solution were imposed. There is significant similarity between the two maps. With the exception of northern Siberia and the central Pacific the location and size of the anomalies are similar.

These results cast a new light on the depth of the origin of the degree 2 anomaly detected by Masters *et al.* (*7*) and confirmed by Woodhouse and Dziewonski (*3*). In those studies it was confined to the transition zone of the upper mantle. Now it seems to be a part of a more complex pattern, varying with radius, but extending across the 670-km discontinuity.

The result shown in Fig. 7 implies the continuity of the anomalies, at least in some locations, but the differential kernels, to the first order, are continuous across the boundary, and smoothing of the solution has been implied by rejecting small eigenvalues of the inner product matrix. What is certain, however, is that the level of heterogeneities in the vicinity of the 670-km discontinuity is elevated in comparison with those at 500 and 800 km, thus indicating the existence of dynamically important processes at this boundary.

Lower mantle. The possibility of the existence of velocity anomalies in the lower mantle was pointed out by Julian and Sengupta (*51*), who found that the *P*-wave rays traveling along different paths but having the bottoming point in the same location in the lower mantle tend to have travel-time residuals of the same sign. This observation was followed by systematic inversions with large data sets (*4, 9, 14, 15, 24*) and limited ones (*13, 52*). Clayton and Comer (*14*) and Dziewonski (*15*) used roughly the same data set, but their approach to model parameterization and inversion was entirely different. Hager *et al.* (*10*) found a significant similarity between these two models at degrees 2 and 3 but not for higher degrees.

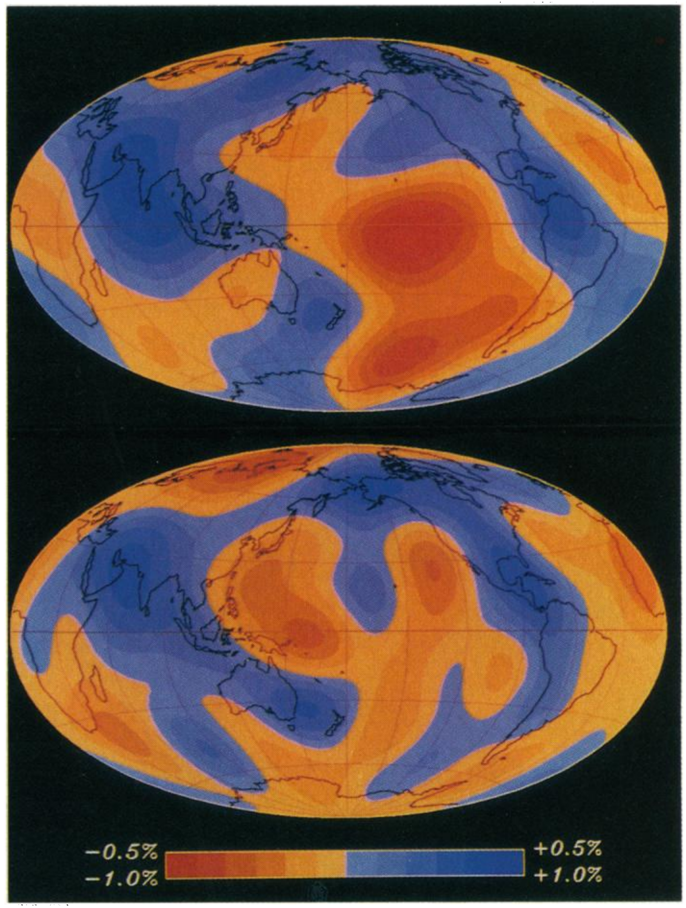

Fig. 8. Maps of the *P*-velocity (top) and *S*-velocity (bottom) anomalies at a depth of 1200 km. The *P*-velocity map contains harmonics up to degree 6 and is calculated from model V3 of Morelli and Dziewonski (*4*) obtained from the analysis of travel-time residuals extracted from BISC (*24*). The *S*-velocity model (harmonics up to degree 8) is U84L85/SH obtained from waveform inversion of about 4000 seismograms (*46*). The correlation between the two maps has a high statistical significance. The range of the relative *S*-velocity perturbations is about twice that of *P*-velocity; note the difference in the color scale.

Recently, Morelli and Dziewonski (*4*) derived model V3 by using a combined set of *P*, *PcP*, *PKP*, and *PKIKP* data extracted from BISC (*21*); in the lower mantle it is similar to L02.56 (*15*). The most striking feature of V3 is the overall slowness of the lower mantle under the Pacific Ocean and relatively high velocities on its rim. The level of heterogeneities is lowest at a depth between 1500 and 2000 km. It begins to increase toward the CMB, but the increase is gradual rather than abrupt, such that it could not be exclusively associated with the anomalous properties of the D″ region, which is located in the lowermost 150 km or so of the mantle.

Some models are derived from data sets other than *P*-wave residuals. There is the *S*-velocity model (*46*), which still has good resolution in the upper part of the lower mantle, and model GLW derived from the analysis of splitting of normal modes (*43*); however, they describe only degrees 2 and 4 of lateral heterogeneity. Figure 8 compares, at a depth of 1200 km, *P*-velocity anomalies of model V3 with *S*-velocity anomalies of model U84L85/SH. The patterns are similar, but the level of relative perturbations in *S*-velocity anomalies is about two times as large as in *P*-velocity, that is, $(\delta v_S/v_S)/(\delta v_P/v_P) \sim 2$. This ratio is much larger than that predicted from laboratory measurements on minerals that are likely constituents of the lower mantle (*53*). Anderson (*54*) shows that this datum has important implications with regard to the thermodynamic properties of terrestrial materials under the temperature and pressure conditions appropriate for the lower mantle.

Figure 9 shows model V3 at a depth of 2300 km; its filtered version, in which only harmonics of degrees 2 and 4 were retained, is shown in the middle panel, and the prediction of model GLW derived from the data on splitting of normal modes is shown at the bottom; the similarity between the two latter maps is striking. Comparing Fig. 9 (middle part) with the splitting function of ${}_1S_7$ in Fig. 4, we find another strong resemblance; since ${}_1S_7$ is principally sensitive to lower mantle *S*-velocity, this indicates a strong relation between heterogeneity in *P* and *S* velocities. Mode ${}_1S_7$ is only one example of modes showing this pattern. The normal mode data also prefer a high $\delta v_S/\delta v_P$ ratio.

A major advantage of modal data is that their sensitivity is not

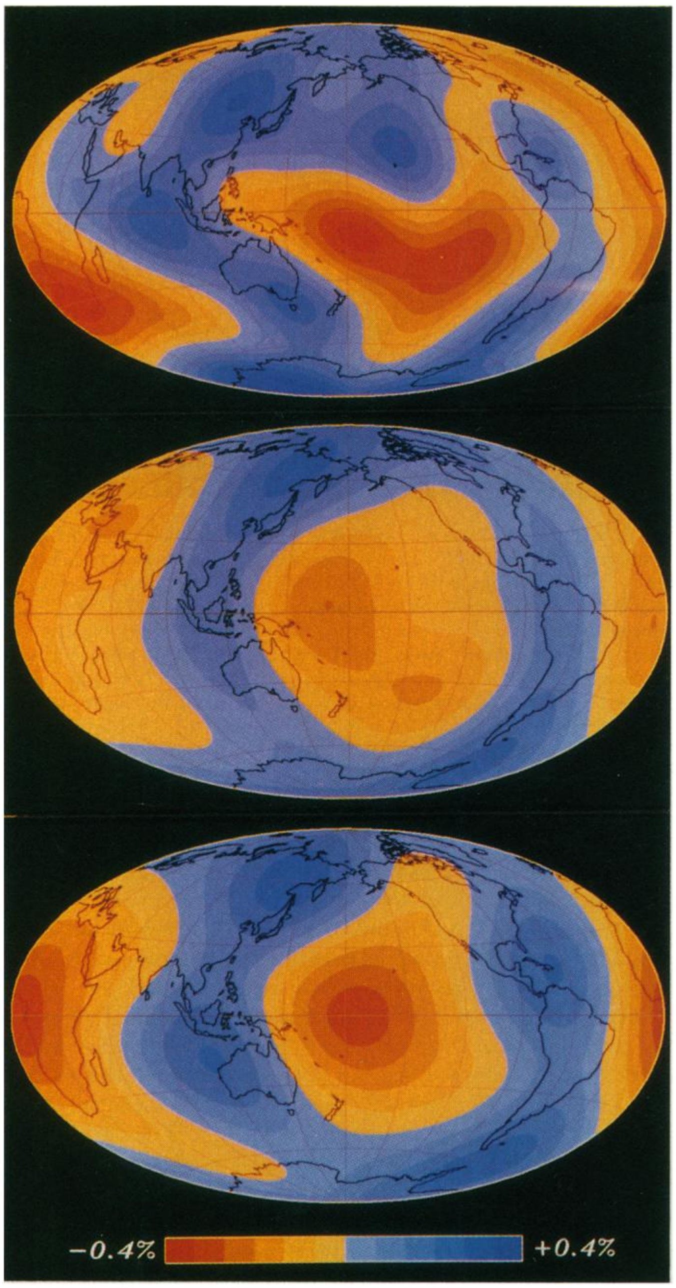

Fig. 9. Comparison of *P*-velocity models derived from travel-time anomalies and splitting of normal models; the depth is 2300 km. The top panel is model V3 (*4*); the same model with only the harmonics of degree 2 and 4 retained is shown in the middle. The bottom panel is from model GLW of Giardini *et al.* (*43*), obtained by inversion of a subset of normal modes. Note that both models at this depth are nearly identical in shape to the splitting function shown in Fig. 4.

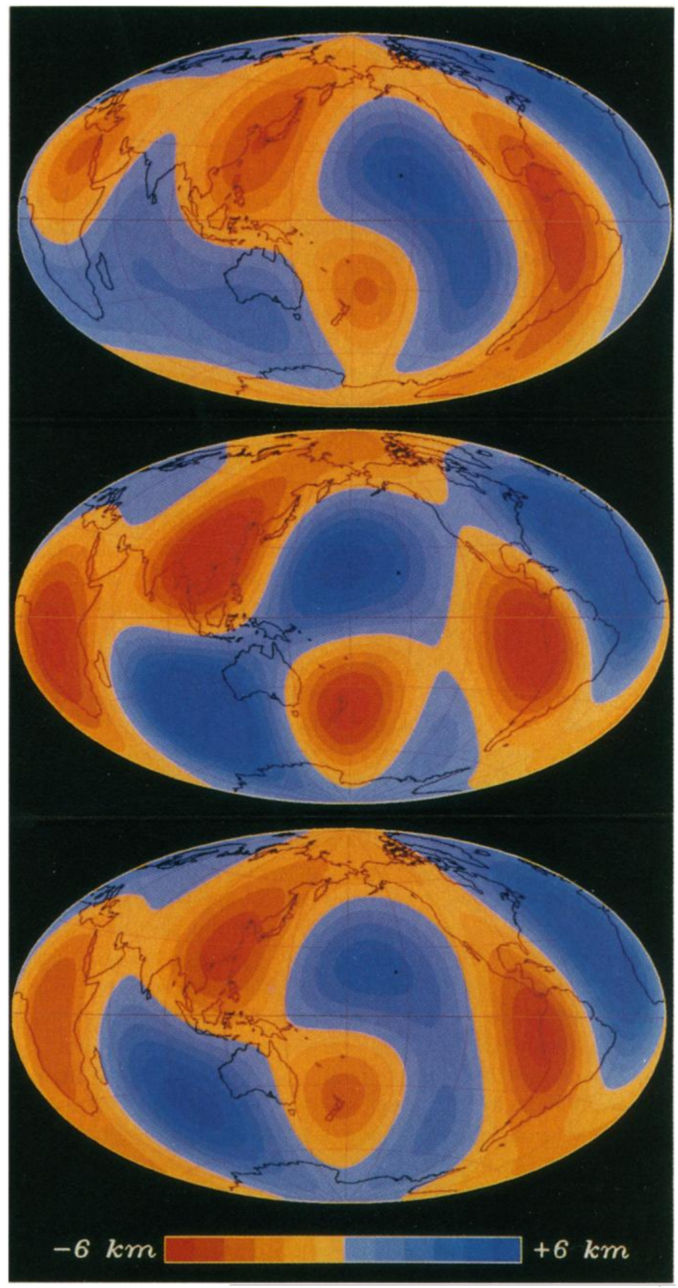

Fig. 10. Topography of the core-mantle boundary from wave travel times in spherical harmonic expansion to degree 4; blue areas are elevated and orange depressed. The top panel shows the result from the analysis of reflections from the core-mantle boundary (*PcP*); middle panel, topography from the anomalies of transmitted waves (PKP_{BC}); bottom panel, result of inversion of the combined *PcP* and PKP_{BC} data set. [Reprinted from (*27*) with permission © Macmillan Journals Ltd.]

limited to the path connecting source and receiver; they provide a way of directly sampling averages over regions of global dimensions. The compatibility of models derived from modal data with models derived from travel times removes the suspicion of distortion due to imperfect global sampling by the body wave data set.

Results such as shown in Figs. 8 and 9 allow us to state that three different data sets yield compatible results for the mantle. These data sets represent different ranges of frequency. The *P*-wave residuals are derived from records that are dominated by 1-Hz energy. The combined waveform data set covers a range of periods from 50 to 300 seconds. The eigenperiods of normal modes used extend from 200 to 1000 seconds. We do not see, therefore, a large frequency dependence over three orders of magnitude in a period.

Core-mantle boundary (CMB) and liquid core. The CMB is the most dramatic discontinuity in the earth's internal structure in terms of the physical and chemical properties as well as the time scale of the processes that take place on either side of it. Its shape, if different from that predicted by the hydrostatic equilibrium theory, may contain information important to our understanding of geodynamic processes in the mantle or the magnetic field generated in the outer core.

The problem has been recently approached by several research groups. Gudmundsson *et al.* (*28*) used *PcP*, a phase reflected from the top of the CMB. Creager and Jordan (*26*) used PKP_{AB} and *PKIKP*, phases transmitted through the boundary. Morelli and Dziewonski (*27*) analyzed both reflected and transmitted data. By using both types of data, we can distinguish between the three hypotheses proposed by Creager and Jordan: (i) the thin, heterogeneous layer above the CMB, (ii) the CMB topography, and (iii) a thin, heterogeneous layer below the CMB. Researchers agree that (i) is inconsistent with the data. Creager and Jordan favor (iii), even though their data cannot distinguish it from (ii); the argument is that a core topography in excess of 10 km is unlikely. Yet, this is the size of the perturbations reported in (*27, 28*).

Figure 10 shows maps of the CMB topography obtained by Morelli and Dziewonski (*27*) using *PcP* (top), PKP_{BC} (middle), and the combined data set (bottom). Since the sensitivities of *PcP* and *PKP* travel times to CMB undulations are of opposite sign, the substantial agreement between the upper two maps—particularly with regard to the sign and location of their extremes—argues strongly that the effects of errors in mantle structure and earthquake locations are small. The resemblance between the *PcP* and *PKP* results is greater in the Northern Hemisphere where data coverage is better.

This experiment also indicates that there is no evidence for a detectable lateral heterogeneity in the outer core, since it would be mapped in the PKP_{BC} results. A large-scale axisymmetric heterogeneity of degree 2 has been proposed by Ritzwoller *et al.* (*42*) as a feature that best explains their results on anomalous splitting of normal modes. Those investigators recognize that the presence of a 0.4% heterogeneity throughout the outer core in a rapidly convecting fluid is unlikely (*55*).

Inner core. Giardini *et al.* (*43*) propose that features in the inner core may account for the properties of modes that are characterized by splitting functions that have large zonal terms of degree 2 and 4, as opposed to those with energy concentrated in the mantle, which are dominated by a P_2^2 pattern (Fig. 4). They show that inner core anisotropy provides a rather natural explanation of anomalous splitting. Poupinet *et al.* (*25*) associated travel-time anomalies of *PKIKP* with the inner core. They proposed a prolate inner core with a polar radius about 100 km greater from the equatorial radius; this model raises questions with regard to its mechanical stability. Evidence of lateral heterogeneity in the inner core on the order of 1% has been reported by Cormier and Choy (*56*). Figure 11A shows the smoothed travel-time anomalies of the *PKIKP* phase

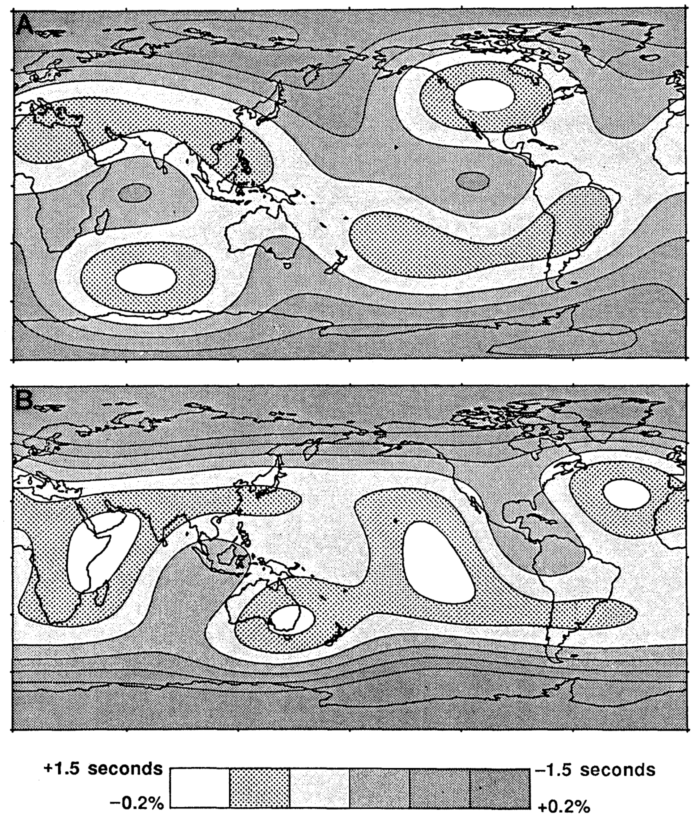

Fig. 11. (**A**) Travel-time anomalies, corrected for lateral heterogeneity above the inner core, of *PKIKP* arrivals at nearly vertical incidence: distance range is 170° to 180°. After Morelli *et al.* (*18*). (**B**) The splitting function for the mode ${}_{13}S_2$; details are in the legend to Fig. 4C. The splitting function is dominated by the axisymmetric terms P_2^0 and P_4^0; the kernels are sensitive to the structure of the inner core. The splitting function of ${}_1S_7$ is dominated by P_2^2, which is present in the lower mantle (Fig. 9). The inference is that lateral heterogeneity in the outer core is not required; the analysis of the travel-time data leads to the same conclusion. After Giardini *et al.* (*43*).

observed between 170° and 180° epicentral distance; such rays travel very close to the center of the earth. There is a strong axisymmetric signature, and the function obtained by the least squares fit of spherical harmonics of degree 0, 2, and 4 has a peak-to-peak amplitude of 2.5 seconds. The data were corrected for lateral heterogeneity in the mantle and for CMB topography. Morelli *et al.* (*18*) were unable to reconcile these observations with the *PKIKP* data at shorter distance ranges (120° to 135° and 155° to 170°), without concentrating the bulk of heterogeneity close to the center of the earth. In addition to implausibility of such a model, it would be inconsistent with the modal data, which indicate that the cause of splitting should be present in the outer part of the inner core. Figure 11B shows the splitting function of the mode ${}_{13}S_2$; a substantial fraction of energy of this mode is in the inner core (*43*). Both maps in Fig. 11 possess large zonal terms; only modes and rays that penetrate deep into the inner core show this effect. Differences between the maps are attributable to the influence of mantle heterogeneity on the modal splitting function.

A hypothesis that seems capable of satisfying travel time and modal data is that the inner core is anisotropic. Morelli *et al.* (*18*) assumed hexagonal anisotropy with the axis of symmetry parallel to the earth's rotation axis. Perturbation in velocity varies then with the angle ξ between the ray and rotation axis as:

$$v(r,\xi) = v_{eq}(r)[1 + \epsilon(r)\cos^2\xi + \sigma(r)\cos^2\xi\sin^2\xi] \qquad (5)$$

where v_{eq} is the velocity in the equatorial plane and ϵ and σ change with radius as $(r/r_{IC})^2$, with r_{IC} being the radius of the inner core.

From the least-squares fit to the data shown in Fig. 11A, Morelli *et al.* obtained $\epsilon = 0.032 \pm 0.005$ and $\sigma = -0.064 \pm 0.015$ (standard errors). Thus, at the surface of the inner core the velocity in the direction parallel to the rotation axis is 3.2% higher than in the equatorial plane. After the data in the three distance ranges are corrected for anisotropy, separate inversions for the "isotropic" heterogeneity lead to consistent results.

Woodhouse *et al.* (*19*) demonstrated that the simple assumption of a constant elastic tensor that is invariant under rotations about the earth's rotation axis (that is, transversely isotropic in the plane of the equator) matches well the gross features of modal observations. Their model does not entirely reconcile the modal data with travel-time observations. They argue, however, that there exists an anisotropic model that will do so.

Discussion

The study of lateral heterogeneity is of great importance to seismology. For example, in investigations of earthquakes the effect of lateral heterogeneity, like an imperfect lens, can distort the image of an event. The estimates of location, fault length, and the pattern of released stresses can be false if the medium is not adequately known. Even the introduction of corrections for low-order lateral heterogeneity can result in shifts of epicenters as much as 20 km and shifts in origin time in excess of 1 second. Although the internal application of three-dimensional modeling is a sort of "housekeeping" problem, which would probably affect only a small circle of experts, the results of global three-dimensional imaging are having an impact on many areas of the geosciences.

The first models of the upper mantle have stimulated the interest of geochemists and petrologists studying planetary scale processes. The three-dimensional models of mid-oceanic ridges, hot spots, and continental roots have profound meaning for the determination of the source and history of the materials found at the surface, which are the only ones that can be studied directly. The evidence from three different studies that v_P and v_S vary systematically with a ratio $(\delta v_S/v_S)/(\delta v_P/v_P)$ between 2 and 2.5 is a new in situ datum for mineral physicists.

The models of the lower mantle have cast new light on the origin of large-scale features in the earth's gravity field, a problem that, in a way, was given up because of the inherent nonuniqueness of the potential field data. It is now clear that the large part of the geoid perturbation originates in the lower mantle (*10*). In addition, by the formulation of the problem in terms of the dynamic response of the earth to an internal load (*57*), it is possible to estimate variations in viscosity with radius.

Seismologists are not the only ones in recent years to produce maps of revolutionary importance. The recovery of secular variations during the last 250 years of the magnetic field at the core-mantle boundary (*58*) may lead to a greatly improved understanding of the geomagnetic secular variation and the geodynamo, one of the

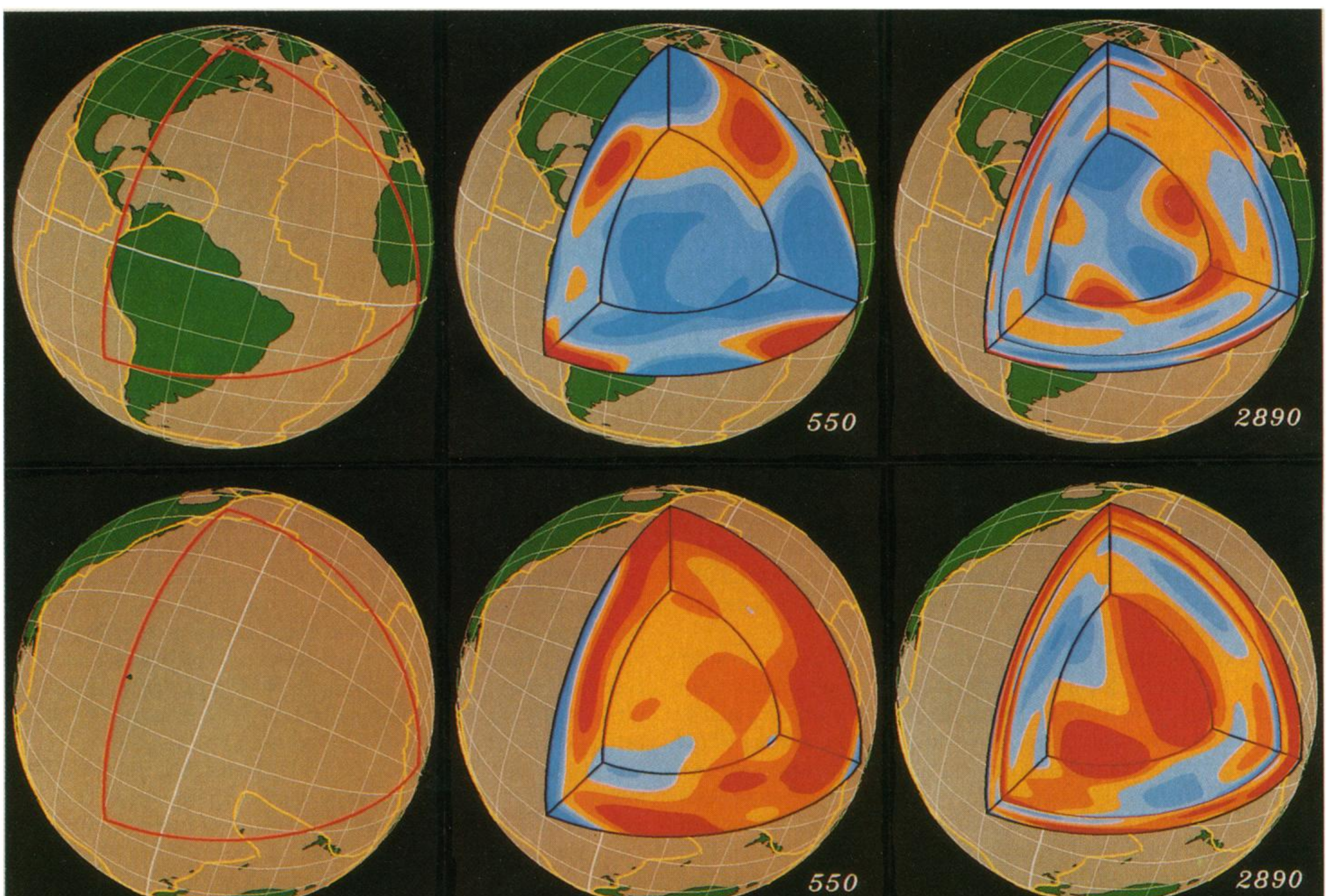

Fig. 12. Windows into the earth. Three-dimensional plots of velocity anomalies under two oceans viewed from an altitude of 35,000 km: the Atlantic (top panels) and the Pacific (bottom panels). Depth to the bottom is indicated in kilometers. In the upper mantle panels (550 km) the depth scale is exaggerated by a factor of 5. Based on models in (*3*) and (*15*). Yellow lines are plate boundaries.

most enigmatic of all geophysical phenomena.

There appears to be significant relation between the space-time pattern of the secular variations and velocity anomalies in the lowermost mantle (*59*). In particular, large static features in the magnetic field, features that are believed to be a direct manifestation of the geodynamo (*60*), appear to be tied to regions of high seismic velocity in the lowermost mantle. This correspondence of magnetic and seismic maps, which is also apparent between regions of proposed upwelling in the core such as beneath southern Africa (*58*) and regions of low seismic velocity, implies thermal coupling between the mantle and flow in the core (*59*). Since the time scale of the mantle processes is many orders of magnitude greater than those in the core, it is possible to infer that the overall pattern of secular variations has been continuing over tens of millions of years.

The anomalous properties of the core-mantle boundary (*26–28*) and the proposed anisotropy in the inner core (*18, 19, 43*)—a hypothesis that requires further verification—are new sources of information that should impose important constraints on the short- and long-term dynamic behavior of the core.

Figure 12 synthesizes the increased capability to view the interior of the earth in a new way. We know from evidence collected at the surface and from the patterns of seismicity that the histories of the Atlantic and Pacific oceans are different. Now we can study these differences all the way to the core-mantle boundary. Without such information it is impossible to understand the earth as a dynamic system.

Some improvements and refinements can be accomplished with the existing data, but the fundamental limitation imposed by the current coverage of the globe with seismographic stations is clear. These limitations are in geographical coverage and in the frequency and amplitude response of the relatively few existing digital stations. In recognition of the broad scientific potential of seismological investigations, a group of U.S. universities founded the Incorporated Research Institutions for Seismology (IRIS) in 1984. The membership of IRIS totals 50 and includes virtually all universities with an active research program in seismology. One of the objectives of IRIS is the establishment of a globally distributed network of permanent seismographic stations with state-of-the-art equipment (*61*). The global network is only a part of the plan. The average distance between stations of an evenly distributed network of 100 observatories is about 2000 km. Such spacing is not sufficient to provide the resolution needed to address specific research problems of planetary implications, be it the question of the penetration of slabs into the lower mantle, details of the structure at the core-mantle boundary, or the sharpness of the transition between the liquid outer core and the solid inner core. Therefore, a set of movable instruments, which would be deployed for a limited time, would be an important complement to the global base of permanent stations.

Parallel initiatives originated in Western Europe (*62*), in particular, in France. A network designed and deployed by French universities, GEOSCOPE (*63*), began operating in 1983 and now has 14 stations distributed worldwide. An international Federation of Broad-Band Digital Seismographic Networks was formed in 1986 with an initial membership of seven countries. The principal objectives of the federation are to ensure the compatibility of the instrumentation used by the member networks and the timely exchange of data (*64*).

The U.S. contribution to the Global Seismographic Network is included in the Global Geosciences initiative of the National Science Foundation. The significance of the network for monitoring and studying catastrophic events such as earthquakes, tsunami waves, volcanic eruptions, and underwater slides makes it a likely candidate for one of the early projects of the International Geosphere-Biosphere Project of the International Council of Scientific Unions.

REFERENCES AND NOTES

1. R. D. Oldham, *J. Geol. Soc. (London)* **62**, 456 (1906); I. Lehmann, *Bur. Cent. Seism. Int.* **A14**, 3 (1936); A. M. Dziewonski and F. Gilbert, *Nature (London)* **234**, 465 (1971). The suggestion that the inner core may be solid was first made by F. Birch [*Am. J. Sci.* **238**, 192 (1940)]. A nearly correct estimate of shear velocity and Poisson ratio for the inner core, based on the assumption of continuity of density and bulk modulus across the inner-outer core boundary, was made nearly 20 years before the eigenfrequencies of several normal modes that are highly sensitive to inner core structure were properly determined [F. Birch, *J. Geophys. Res.* **57**, 227 (1952); see also K. E. Bullen, *Nature (London)* **157**, 405 (1946); B. Bolt, *Bull. Seismol. Soc. Am.* **54**, 191 (1964); D. L. Anderson, C. Sammis, T. Jordan, *Science* **171**, 1103 (1971)].
2. H.-C. Nataf, I. Nakanishi, D. L. Anderson, *Geophys. Res. Lett.* **11**, 109 (1984).
3. J. H. Woodhouse and A. M. Dziewonski, *J. Geophys. Res.* **89**, 5953 (1984).
4. A. Morelli and A. M. Dziewonski, *Eos* **67**, 311 (1986).
5. X.-D. Li, D. Giardini, J. H. Woodhouse, *ibid.*, p. 307.
6. D. Agnew, J. Berger, R. Buland, W. Farrell, F. Gilbert, *ibid.* **57**, 180 (1976); J. Peterson, H. M. Butler, L. G. Holcomb, C. R. Hutt, *Bull. Seismol. Soc. Am.* **66**, 2049 (1976).
7. G. Masters, T. H. Jordan, P. G. Silver, F. Gilbert, *Nature (London)* **298**, 609 (1982).
8. I. Nakanishi and D. L. Anderson, *Bull. Seismol. Soc. Am.* **72**, 1185 (1982).
9. A. M. Dziewonski, B. H. Hager, R. J. O'Connell, *J. Geophys. Res.* **82**, 239 (1977).
10. B. H. Hager, R. W. Clayton, M. A. Richards, R. P. Comer, A. M. Dziewonski, *Nature (London)* **313**, 541 (1985).
11. T. H. Jordan, *Rev. Geophys. Space Phys.* **13**, 1 (1975); *Nature (London)* **274**, 544 (1978).
12. ———, *J. Geophys.* **43**, 473 (1977); K. C. Creager and T. H. Jordan, *J. Geophys. Res.* **89**, 3031 (1984).
13. M. K. Sengupta and M. N. Toksöz, *Geophys. Res. Lett.* **3**, 84 (1976).
14. R. W. Clayton and R. P. Comer, *Eos* **64**, 776 (1983).
15. A. M. Dziewonski, *J. Geophys. Res.* **89**, 5929 (1984).
16. T. Tanimoto, *Geophys. J. R. Astron. Soc.* **82**, 105 (1985); *ibid.* **84**, 46 (1986).
17. G. E. Backus and F. Gilbert, *ibid.* **16**, 169 (1968); *Philos. Trans. R. Soc. London Ser. A* **266**, 123 (1970).
18. A. Morelli, A. M. Dziewonski, J. H. Woodhouse, *Geophys. Res. Lett.* **13**, 1545 (1986).
19. J. H. Woodhouse, D. Giardini, X.-D. Li, *ibid.*, p. 1549.
20. C. R. Gwinn, T. A. Herring, I. I. Shapiro, *J. Geophys. Res.* **91**, 4755 (1986); J. M. Wahr, *Geophys. J. R. Astron. Soc.* **88**, 265 (1987).
21. *Bulletin of the International Seismological Centre: Catalogue of Events and Associated Observations* (years 1964–1983), vols. 1–20 (International Seismological Centre, Newbury, Berkshire, England, 1967–1986).
22. W. L. Donn, *The Earth* (Wiley, New York, 1972).
23. A. M. Dziewonski, *Eos* **56**, 395 (1975).
24. A. Morelli and A. M. Dziewonski, *ibid.* **66**, 975 (1985). When summary *P*-wave residuals, with data available for some 68,000 source-receiver pairs, are sorted by the number of observations, N, used to derive the average, the variance estimate σ_N^2 of single observation within each such population shows dependence on N. For N between 1 and 30 this may be modeled, with a root mean square of $0.02s^2$, by: $\sigma_N^2 = \sigma_r^2/N + \sigma_c^2$, where σ_r^2 is about $2s^2$ and σ_c^2 is $0.2s^2$. The inference is that the term σ_r^2/N is due to random noise and modeling should be restricted to attempts to reduce σ_c^2.
25. G. Poupinet, R. Pillet, A. Souriau, *Nature (London)* **305**, 204 (1983).
26. K. C. Creager and T. H. Jordan, *Geophys. Res. Lett.* **13**, 1497 (1986).
27. A. Morelli and A. M. Dziewonski, *Nature (London)*, **325**, 678 (1987).
28. O. Gudmundsson, R. W. Clayton, D. L. Anderson, *Eos* **67**, 1100 (1986).
29. H.-W. Zhou and R. W. Clayton, *ibid.* **66**, 975 (1985); J. H. Davies and R. W. Clayton, *ibid.* **67**, 1099 (1986).
30. I. Nakanishi and D. L. Anderson, *Geophys. J. R. Astron. Soc.* **78**, 573 (1984).
31. H.-C. Nataf, I. Nakanishi, D. L. Anderson, *J. Geophys. Res.* **91**, 7261 (1986).
32. D. L. Anderson and A. M. Dziewonski, *Geophys. J. R. Astron. Soc.* **69**, 383 (1982).
33. T. Tanimoto and D. L. Anderson, *Geophys. Res. Lett.* **11**, 287 (1984); *J. Geophys. Res.* **90**, 1842 (1985).
34. T. Tanimoto, *Eos* **67**, 1099 (1986).
35. N. Jobert, R. Gaulon, A. Dieulin, G. Roult, *C. R. Acad. Sci. Paris* **B285**, 49 (1977); E. A. Okal and B.-G. Jo, *Geophys. Res. Lett.* **12**, 421 (1985).
36. G. E. Backus and F. Gilbert, *Proc. Natl. Acad. Sci. U.S.A.* **47**, 362 (1961); C. L. Pekeris, Z. Alterman, M. Jarosch, *Phys. Rev.* **122**, 1692 (1961); F. A. Dahlen, *Geophys. J. R. Astron. Soc.* **16**, 329 (1968); B. N. Zharkov and V. M. Lyubimov, *Izv. Acad. Sci. USSR Phys. Solid Earth* **10**, 613 (1970); R. Madariaga and K. Aki, *J. Geophys. Res.* **77**, 4421 (1972); F. A. Dahlen, *Geophys. J. R. Astron. Soc.* **44**, 77 (1976).
37. T. H. Jordan, *Geophys. J. R. Astron. Soc.* **52**, 441 (1978); J. H. Woodhouse and T. P. Girnius, *ibid.* **68**, 653 (1982); F. A. Dahlen, *ibid.* **58**, 1 (1979).
38. H. Benioff, F. Press, S. W. Smith, *J. Geophys. Res.* **66**, 605 (1961); N. F. Ness, C. S. Harrison, L. J. Slichter, *ibid.*, p. 621.
39. R. Buland, J. Berger, F. Gilbert, *Nature (London)* **277**, 358 (1979).
40. G. Masters and F. Gilbert, *Geophys. Res. Lett.* **8**, 569 (1981).
41. A. M. Dziewonski and F. Gilbert, *Geophys. J. R. Astron. Soc.* **35**, 401 (1973); R. S. Anderssen, J. R. Cleary, A. M. Dziewonski, *ibid.* **43**, 1001 (1975); F. Gilbert, *ibid.*, p. 1007.
42. M. Ritzwoller and G. Masters, *Eos* **65**, 1003 (1984); ———, F. Gilbert, *ibid.* **66**, 966 (1985); *J. Geophys. Res.* **91**, 10203 (1986).
43. D. Giardini, X.-D. Li, J. H. Woodhouse, *Nature (London)* **325**, 405 (1987).
44. J. Woodhouse and D. Giardini, *Eos* **66**, 300 (1985).
45. A. M. Dziewonski and D. L. Anderson, *Phys. Earth Planet. Inter.* **25**, 297 (1981).
46. J. H. Woodhouse and A. M. Dziewonski, *Eos* **67**, 307 (1986).
47. J. Brune and J. Dorman, *Bull. Seismol. Soc. Am.* **53**, 167 (1963); B. J. Mitchell and G.-K. Yu, *Geophys. J. R. Astron. Soc.* **63**, 497 (1980); A. R. Leeds, L. Knopoff, E. G. Kausel, *Science* **186**, 141 (1974).
48. B. H. Hager and R. J. O'Connell, *J. Geophys. Res.* **84**, 1031 (1979).

49. D. L. Anderson and M. N. Toksöz, *ibid.* **68**, 3483 (1963); L. R. Johnson, *ibid.* **72**, 6309 (1967); P. G. Richards, *J. Geophys.* **38**, 517 (1972); A. C. Lees, M. S. T. Bukowinski, R. Jeanloz, *J. Geophys. Res.* **88**, 8145 (1983).
50. Abstracts from a session on "Deep slab penetration" at the 1986 spring meeting of the American Geophysical Union [*Eos* 67, 379 and 380 (1986)].
51. B. R. Julian and M. K. Sengupta, *Nature (London)* **242**, 443 (1973).
52. M. K. Sengupta, R. E. Hassel, R. W. Ward, *J. Geophys. Res.* **86**, 3913 (1981).
53. O. L. Anderson, E. Schreiber, R. C. Lieberman, M. Soga, *Rev. Geophys. Space Phys.* 6, 491 (1968).
54. D. L. Anderson, *Phys. Earth Planet. Inter.*, in press.
55. D. Stevenson, *Geophys. J. R. Astron. Soc.* **88**, 311 (1987).
56. V. F. Cormier and G. L. Choy, *Geophys. Res. Lett.* **13**, 1553 (1986).
57. M. A. Richards and B. H. Hager, *J. Geophys. Res.* **89**, 5987 (1984).
58. J. Bloxham and D. Gubbins, *Nature (London)* **317**, 777 (1985).
59. _____, *ibid.*, **325**, 511 (1987).
60. D. Gubbins and J. Bloxham, *ibid.*, p. 509.
61. *Science Plan for New Global Seismographic Network* (Incorporated Research Institutions for Seismology, Washington, DC, 1984); S. W. Smith, *Eos* 67, 213 (1986).
62. G. Nolet, B. Romanowicz, R. Kind, E. Wielandt, *ORFEUS Science Plan* (Reidel, Dordrecht, Netherlands, 1986).
63. B. Romanowicz, M. Cara, J. F. Fels, D. Rouland, *Eos* 65, 753 (1984).
64. B. Romanowicz and A. M. Dziewonski, *ibid.* 67, 541 (1986).
65. We thank J. Bloxham, D. Giardini, X.-D. Li, and A. Morelli for discussions and D. L. Anderson for suggestions on the manuscript. Some results and figures are from unpublished research in which D. Giardini, X.-D. Li, and A. Morelli were our co-workers. We thank D. Stevenson (*55*) for a preprint. Research described here was made possible by the bulletin data compiled by the International Seismological Centre and digital recordings from two networks: Global Digital Seismographic Network operated by the U.S. Geological Survey and the International Deployment of Accelerometers operated by the University of California, San Diego. Supported by the National Science Foundation under grants EAR81-20944, EAR82-13330, EAR83-17594, EAR84-18332, and EAR85-11400.

Gene Transfer in Crop Improvement

ROBERT M. GOODMAN, HOLLY HAUPTLI, ANNE CROSSWAY, VIC C. KNAUF

Transfer of genes between plant species has played an important role in crop improvement for many decades. Useful traits such as resistance to disease, insects, and stress have been transferred to crop varieties from noncultivated plants. Recombinant DNA methods greatly extend (even outside the plant kingdom) the sources from which genetic information can be obtained for crop improvement. Gene transfer systems based on recombinant DNA are available for several crop species and are under development for others. The concerted use of traditional and more recent methods for plant genetic manipulation will contribute to crop improvement.

RAPID PROGRESS IS BEING MADE IN DEVELOPING THE tools for manipulating genetic information in plants by recombinant DNA methods. Plant genes are being cloned, genetic regulatory signals deciphered, and genes transferred from entirely unrelated organisms (notably bacteria and a virus) to confer new agriculturally useful traits on crop plants. Recombinant DNA methods significantly increase the gene pool accessible for crop improvement.

In this review we summarize and illustrate with selected examples the long history of gene transfer by plant breeders between plant species and even between plants from different genera. We describe the use of recombinant DNA–based methods for gene transfer to plants and indicate with examples how these may contribute to the future of crop improvement. Our analysis highlights the important role continuing development of technology (Fig. 1) has played in expanding the range of organisms from which genetic information can be mobilized to plants. We conclude with some views on issues related to the use of technology in crop improvement and the future strength of agriculture.

R. M. Goodman is executive vice president, research and development; H. Hauptli is principal scientist; A. Crossway is managing scientist; and V. C. Knauf is managing scientist, at Calgene, Inc., Davis, CA 95616.

Gene Transfer Through Hybridization

Plant breeding and intraspecific gene transfer. Plant breeding as a science began in the 19th century with discoveries of how plant traits are inherited (*1*). The early years saw transfer and reassortment of large numbers of genes in heterogeneous cultivated populations (landraces). Breeders steadily expanded their search for new genetic variation to the entire crop species, including noncultivated populations. These were gene transfers within the species. It is from such exchanges that our modern cultivated varieties originated (*2*). Often, however, the crop species does not contain sufficient genetic diversity to allow the desired improvements. The search for added diversity has been a stimulus for plant breeders to adopt new technology.

In simple terms, plant breeding is the selection of plants with desired traits after the sexual exchange of genes by cross-fertilization between two parents. When one parent is a cultivated variety and the other a wild relative, an improved variety is formed by back-crossing to the cultivated parent and selecting for the desired combinations of characteristics. Plant breeding has developed into a sophisticated science, aided in part by the application of statistical tools. The alliance of genetics with probability theory has allowed plant geneticists to arrive at more efficient models for the combination and selection of genes in populations and breeding lines. Statistical methods are now indispensable in the design of field experiments and in the prediction and analysis of results (*1*).

The definition of a plant species rests on the concept of genetic isolation. Nevertheless, sexual exchange of genes between species can and does occur in nature without human intervention. One of the better documented cases of such transfer is that between maize (*Zea mays*) and teosinte (*Z. mexicana*) (*3*). Use by plant breeders of sexual exchanges between species as sources of genetic variability to improve crops has been made possible during the past 80 years by the discovery of efficient ways to circumvent the natural barriers to genetic exchange by sexual mechanisms.

Interspecific gene transfer. For certain crops, plant breeders in the 20th century have increasingly used interspecific hybridization for the transfer of genes from a noncultivated plant species to a crop variety in a related species (Table 1). The exploitation of interspecif-